RESEARCH ARTICLE

Decoupling and Cloaking of Tailored Complementary Cloaked Antennas

DOOJIN LEE , (Member, IEEE)

Department of Electrical, Electronic, and Control Engineering, Changwon National University (CWNU), Changwon 51140, South Korea

e-mail: doojin.lee@changwon.ac.kr

ABSTRACT We explore complementary cloaked antennas to improve their designs and to increase our understanding of the fundamental concepts of mutual coupling and cloaking effects by metasurface cloaks. We show that a cloaked planar dipole antenna (CPDA) and a cylindrically grounded cloaked slot antenna (CGCSA) placed in close proximity can be decoupled in the near field and cloaked in the far field of using planar metasurface cloaks; the antennas operate as if they were isolated. We perform an intensive parametric study to determine the optimal decoupling and cloaking regimes for both the CPDA and the CGCSA. The structures developed are in good agreement with previous findings regarding the cloaking effects, even when complementary antennas are in close proximity. Such analysis can also be applied to other types of complementary antennas placed close together that operate in neighboring frequency bands.

INDEX TERMS Cloaking, complementary structure, metasurface, planar antennas, slot antennas, scattering cancellation.

I. INTRODUCTION

Cloaks are designed to make targets invisible or concealed over specific spectral ranges of electromagnetic waves [1], [2], [3], [4], [5]. Cloaking has many applications in the industrial and defense fields. In terms of defense, the survival of military forces is the main priority in the modern electronic warfare. Self-defense systems use cloaks to protect electronic equipment from electromagnetic waves emitted by enemy radar. The demand for high-end cloaking is growing; there is a need to minimize the total scattering cross-section.

In addition to defense, cloaks are in high demand in the communications field; they are also in demand for electronic devices in very dense environment [6], [7]. The many onboard electronic devices used by modern methods of transport require multiple antennas to be mounted on a compact platform; all simultaneously operate within a narrow spectrum. The main problem is the inevitable electromagnetic interference that occurs when many antennas are closely packed [7], [8]. This interference degrades overall performances; radiations from adjacent antennas strongly interfere, considering their subwavelength separation [6], [7], [8].Cloaking decouples such interference.

The associate editor coordinating the review of this manuscript and approving it for publication was Ladislau Matekovits .

The fundamental principles are well established; guided wave cloaks and scattering cancellation methods have been extensively studied [9], [10], [11], [12], [13], [14], [15], [16], [17], [18], [19], [20], [21], [22], [23]. A guided wave cloak is essentially a shell that directs waves away from the cloaked target [12], [13], [14], [15], [16]. The waves bend around the target, passing through well-defined transformative optics-based metamaterials [12], [13], [14], [15], [16]. Guided wave cloaks include transmission-line based cloaks [17], [18], [19], [20], a series of metallic layers that guide waves around targets [17], [18], [19], [20]. These layers are coupled with free space during impedance matching processes. A cloak is formed through interactions within the layers [17], [18]. However, practical applications are difficult [1], [2], [3], [4] [6], [7] because guided wave cloaks occupy substantial volumes through which cloaked waves are detoured [12], [13], [14], [15], [16]. Additionally, the high dielectric and conduction losses reduce efficiency.

Scattering cancellation cloaks use metamaterials or metasurfaces that cause fields to mutually cancel [1], [2], [3], [4], [5], [6], [7], [8]. Thus, a field scattered by the target to be cloaked is successfully canceled by a field that has been created using a specifically designed material [1], [2], [3], [4], [5], [6], [7], [8]. The metamaterial or metasurface generates a destructive fields, which is the exact opposite of the scattering

field re-radiated from the target [1], [2], [3], [4], [5], [6], [7], [8]. However, plasmonic cloaks use cumbersome media, such as plasmonic metamaterials with negative relative dielectric constants that restrain fields scattered by the target [9], [10], [11]. The size of plasmonic cloaks are typically comparable with the sizes of the target [9], [10], [11].

Mantle cloaking involves an ultra-thin metasurface [1], [2], [3], [4], [5], [6], [7], [8]. Such cloaking is based on scattering cancellation by a super-thin metasurface surrounding the target [1], [2], [3], [4]. The mechanism is electrical; the cancelling field is induced by anti-phase metasurface currents. Extensive analytical and numerical studies using dielectric and conducting cylindrical objects have appeared [6], [21]. Various super-thin one-or two-dimensional (2D) metasurfaces have been conformally printed and placed in slotted arrays that are periodically arranged at sub-microwave frequencies [21]. Such scattering cancellation method has also been implemented at low-THz frequencies using an ultra-thin graphene layer [3]. Mantle cloaking in the microwave region has been intensively studied; elliptical metasurfaces were used to surround bare metallic monopole or dipole antennas in [1] and wideband cloaked antennas in [2]. These studies were then extended to interleaved antenna arrays with the antenna elements in close proximity and operating at neighboring frequencies [4], [7], [8]. The performance of cross-coupled, printed, monopole antenna arrays surrounded by elliptical metasurfaces was explored in [8], whereas the performance of printed dipole antenna was explored in [7]; interference caused by the radiations of adjacent antennas was eliminated.

A planar cloaking metasurface in which an anti-phase current traveled was recently proposed for a bowtie antenna [7]. This approach suggests that planar metasurfaces can be directly applied during planar antenna printing, even with respect to antennas that exhibit electrically large dimensions (approximately one half-wavelength). Recently, mantle cloaking has been successfully implemented for slot antennas operating at C-band frequencies [22], [23]. An elliptical metasurface was placed at the edge of the slot aperture. Scattering was cancelled. This eliminated mutual coupling that involved a neighboring slot antenna operating in the C-band.

Inspired by the findings of [22] and [23], the present study explores the fundamentals of mantle cloaking, as well as the decoupling effects of complementary antennas. We show that a cloaked planar dipole antenna (CPDA) and a complementary, cylindrically grounded, cloaked slot antenna (CGCSA) placed in close proximity are decoupled in the near field but cloaked in the far field; the complementary antennas then operate as if they were isolated.

II. COMPLEMENTARY CLOAKED ANTENNAS
A. TAILORED COMPLEMENTARY ANTENNAS
We study the complementary cloaked antennas, CPDA and CGCSA, shown in Figure. 1. The complementary structure is guided by the Babinet's principle of optics. Thus,
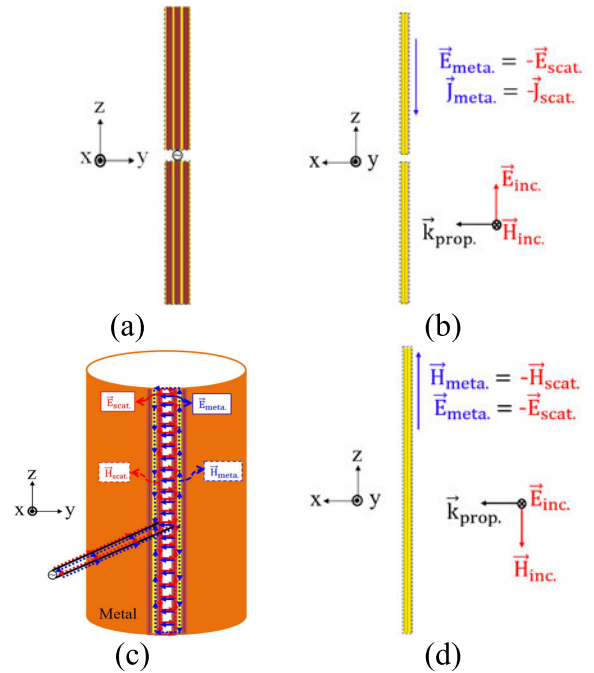

FIGURE 1. Schematic representation of tailored complementary structure of cloaked antennas: (a) CPDA in the YOZ-plane, (b) CPDA in the XOZ-plane, (c) CGCSA in the YOZ-plane, and (d) CGCSA in the XOZ-plane.

a metallic dipole strip antenna in free space is precisely the dual structure of a slot antenna surrounded by an infinite metal sheet. Considering this background sheet, the antenna input impedance between complementary structures satisfies the condition $Z_d \cdot Z_s = \eta_0^2/4$, where Z_d, Z_s, and η_0 are the input impedances of the metallic dipole and slot antennas, and the intrinsic impedance in free space, respectively. Here, we use the cylindrically grounded, cloaked slot antenna CGCSA, shown in Figure 1(c) and (d), to practically represent the ground plane. Accordingly, the cylindrically grounded structure can be regarded as the continuous, background metallic sheet that facilitates radiation from the slot antenna.

Consider a cloaked planar dipole antenna (CPDA) with a transverse magnetic polarized (TM^z) incident wave that impinges with respect to the z-axis as shown in Figure. 1(a) and (b). This wave can be represented as fields that engage in electromagnetic interference at the CPDA operating frequency. When the incident wave reaches the CPDA, an anti-phase current is created by the metasurface impedance; thus, it is directly induced on the metasurface to cancel the fields scattering from the bare antenna. This scenario can be formulated as:

$$\vec{E}_{meta.} = Z_{meta.} \cdot \vec{J}_{meta.} = -\vec{E}_{scat.} \qquad (1)$$

where $\vec{E}_{meta.}$, $Z_{meta.}$, $\vec{J}_{meta.}$, and $\vec{E}_{scat.}$ are the electric field created on the metasurface, surface impedance of the metasurface, current density on the metasurface, and the electric field scattering from the bare antenna, respectively. The surface impedance of the metasurface ($Z_{meta.}$) must be carefully chosen to induce the required anti-phase current. Generally,
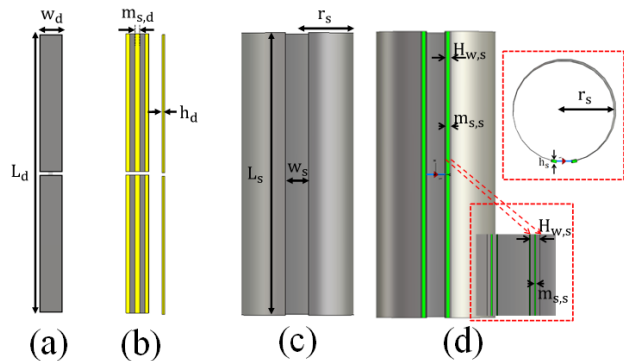
FIGURE 2. Configurations of (a) uncloaked planar dipole antenna, (b) cloaked planar dipole antenna (CPDA), (c) cylindrically grounded uncloaked slot antenna, and (d) cylindrically grounded cloaked slot antenna (CGCSA).

FIGURE 3. Characteristics of uncloaked complementary antennas: (a) reflection coefficient and (b) total efficiencies by frequency.

FIGURE 4. Characteristic variations of the CPDA as the dielectric constant ($\varepsilon_{r,d}$) changes: (a) reflection coefficient and (b) total efficiency according to frequency.

FIGURE 5. Parametric study of the CPDA as the height of the metasurface host material (h_d) is varied: (a) reflection coefficient and (b) total efficiency.

the reactance of $Z_{meta.}$ should be positive for a dielectric object, which is inherently capacitive; it should be negative for a conducting object, which is inherently inductive. Here, the bare antenna is inductive; thus, the reactance of the metasurface should be negative. Then, the CPDA is almost cloaked against the incident wave and the operating frequency is not affected by that wave.

Similarly, assume that a transverse electric polarized (TE^z) wave is incident [Fig. 1(d)] to the cylindrically grounded, cloaked slot antenna (CGCSA), thereby comprising the dual structure of the CPDA. Here, a reverse E-field is induced at the edge of the slot metasurface when the TE^z- polarized wave reaches the structure. A magnetic field around the metasurface is then created in the direction opposite to the scattering magnetic field. This arrangement cancels the field and thus cloaks the slot antenna. Mathematically:

$$\vec{H}_{meat.} = Y_{meat.} \cdot \vec{E}_{meat.} = -\vec{H}_{scat.} \qquad (2)$$

where $\vec{H}_{meta.}$, $Y_{meta.}$, $\vec{E}_{meta.}$, and $\vec{H}_{scat.}$ are the magnetic field created on the metasurface, the surface admittance of the metasurface, the electric field on the metasurface, and the magnetic field scattered from the uncloaked slot antenna, respectively.

B. METASURFACE-CLOAKED ANTENNAS

Both the uncloaked planar dipole antenna and the cylindrically grounded uncloaked slot antenna initially operate at approximately 3.2 GHz. The configuration of the uncloaked planar dipole antenna and the CPDA are shown in Figure 2(a) and (b) respectively. The cylindrically grounded uncloaked slot antenna and CGCSA are illustrated in Figure. 2(c) and (d), respectively. These antennas were designed with the aid of the CST Studio Suite (CST-Microwave Studio) [24]. The length (L_d) and width (w_d) of the dipole, uncloaked planar antenna of Figure 2(a) are 43mm and 3.5mm, respectively. We assumed that the length (L_s) and width (w_s) of the slot of the cylindrically grounded, uncloaked slot antenna exhibited the same
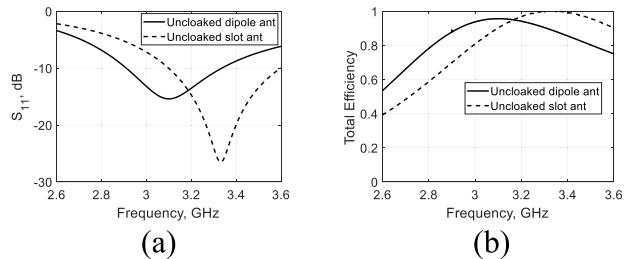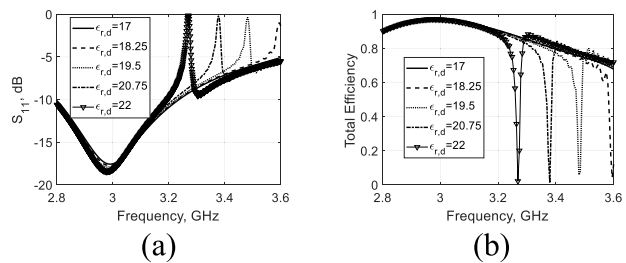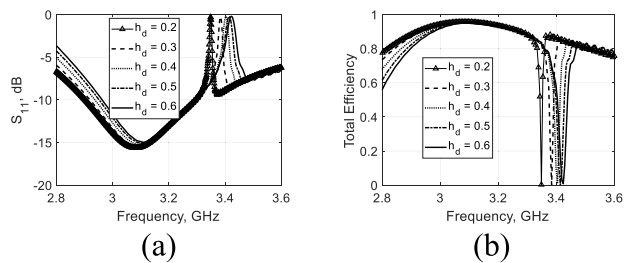
dimensions. The radius of the cylinder is $\lambda_0/10$, where λ_0 is the wavelength at 3.2 GHz.

Figure 3(a)-(b) shows the scattering parameter and total efficiencies of the uncloaked complementary antennas. The reflection coefficients of the uncloaked dipole and slot antenna [Fig. 3(a)] are similar near 3.2GHz. Thus, the resonance frequency is 3.1 GHz for the uncloaked planar dipole antenna and 3.3 GHz for the cylindrically grounded uncloaked slot antenna. The parametric study was performed by varying the dielectric constant of the metasurface host material ($\varepsilon_{r,d}$) [Figs. 4(a)-(b)]. As $\varepsilon_{r,d}$ increases, the cloaked frequency shifts lower. Figure 4(a) shows the reflection coefficient curve, whereas Figure 4(b) shows the total efficiency. The guided wavelength becomes shorter. The current then runs through a longer path than the path imposed by the physical limitation of the antenna; thus, the cloaked frequency is shifted lower as $\varepsilon_{r,d}$ increases.

The height of the host material (h_d) was explored by varying h_d only. The curve characteristics at cloaked frequencies,
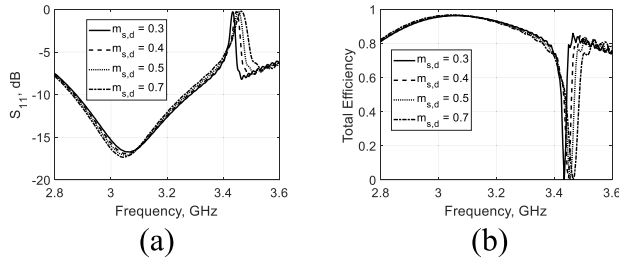
FIGURE 6. Characteristic CPDA variations as functions of frequency when the metasurface slot ($m_{s,d}$) is varied: (a) reflection coefficient and (b) total efficiency.
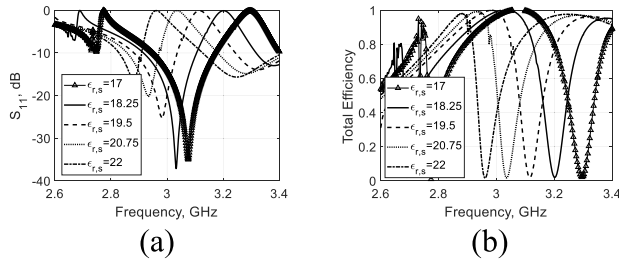

FIGURE 7. Characteristic changes in the dielectric constant of the CGCSA host ($\varepsilon_{r,s}$): (a) reflection coefficient and (b) total efficiency.

FIGURE 8. The (a) reflection coefficient and (b) total efficiency with respect to the changes in the host metasurface width ($H_{w,s}$).

FIGURE 9. (a) Reflection coefficient and (b) total efficiency as the height of the host material (h_s) is varied.

FIGURE 10. The (a) reflection coefficient and (b) total efficiency as the metasurface surface slot ($m_{S,s}$) changes.

thus the reflection coefficient of Figure 5(a) and total efficiency of Figure 5 (b), shit toward higher frequencies as h_d increases because the total capacitance decreases as h_d increases.

Figure 6(a)-(b) show the changes in the characteristics as the metasurface slot ($m_{s,d}$ value) varies. As $m_{s,d}$ increases, the cloaked frequency increases in terms of the reflection coefficient [Fig. 6(a)] and total efficiency [Fig. 6(b)] because the total capacitances decrease, shifting the cloaked frequency higher as $m_{s,d}$ increases.

The cloaked slot structure of our CGCSA is based on the structure described in [22] and [23], but it includes a planar cloaked host at the edge of the slot. The detailed metasurface parameters of Figure 2(c) are: the dielectric constant of the host material ($\varepsilon_{r,s}$), the height of the host material (h_s), the size of the slot on the metasurface ($m_{s,s}$), and the host width of the metasurface ($H_{w,s}$).

Figure 7(a)-(b) shows the changes in the characteristics—reflection coefficient [Fig.7 (a)] and total efficiency [Fig. 7(b)] —when only $\varepsilon_{r,s}$ changes. As suggested by previous studied, the cloaked frequency, which is 0 dB when the reflection coefficient corresponds to zero total efficiency, shifts toward lower frequencies as $\varepsilon_{r,s}$ increases.

The effect of the metasurface host width ($H_{w,s}$) was explored by varying that value within specific ranges when the other parameters were fixed. As $H_{w,s}$ increases, the cloaked frequency shifts lower for both the reflection coefficient [Fig. 8(a)] and total efficiency [Fig. 8(b)]; as $H_{w,s}$ increases, the total inductances of the series inductors increase, thereby changing the cloaked frequency.
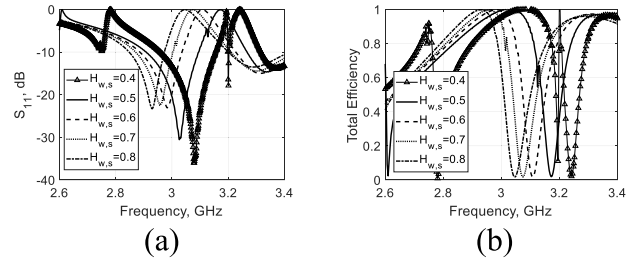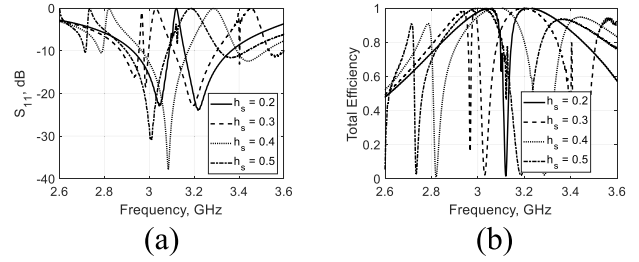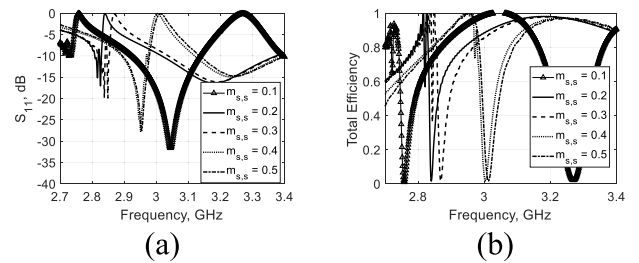
The characteristics of Figure 9(a)-(b) were derived by changing the parameter h_s while the other parameters remained fixed. The cloaked frequencies move lower as h_s increases for both the reflection coefficient curve and the total efficiency because the inductive component becomes more dominant than the capacitive component. Thus, unlike for the CPDA, the width of the host metasurface ($H_{w,s}$) is very similar to the height of the host material (h_s) of the CGCSA.

Figure 10(a)-(b) shows the characteristic changes in the metasurface slot ($m_{s,s}$) of the CGCSA with respect to reflection coefficient and total efficiency. As $m_{s,s}$ increases, the cloaked frequency shifts higher because the total capacitances decreases.

III. CLOAKING AND DECOUPLING OF COMPLEMENARY ANTENNAS
A. PERFORMANCES OF COMPLEMENTARY ANTENNAS
The complementary cloaked antennas (i.e., the CPDA and the CGCSA) were subjected to numerical studies. The final dimensions of the complementary cloaked antennas were:
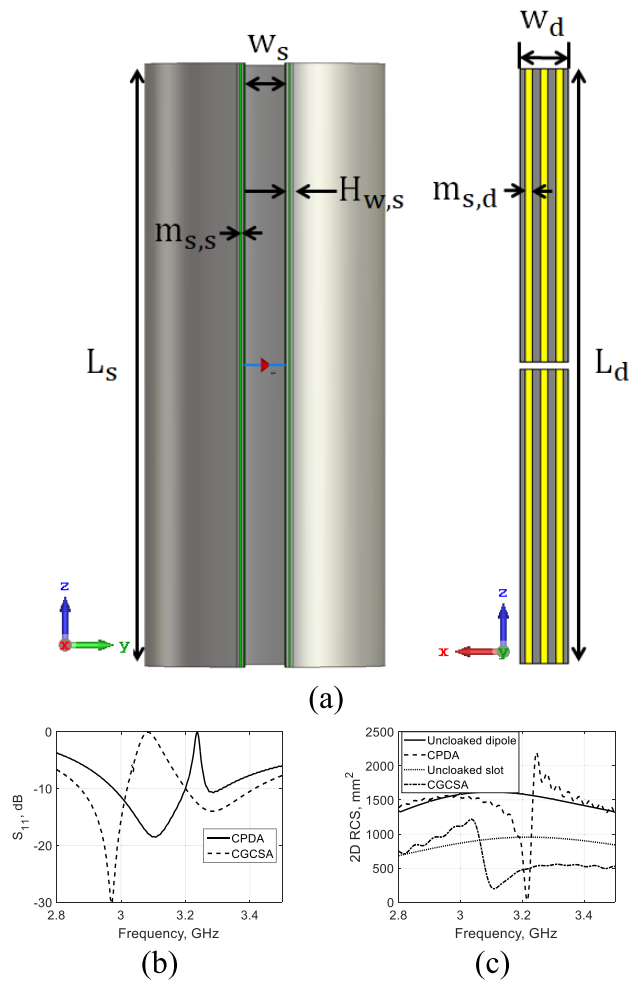
FIGURE 11. Characteristic performances of complementary cloaked antennas according to frequency: (a) final complementary cloaked antennas, (b) reflection coefficient, (c) 2D radar cross-sections (2D-RCS).

$L_d = 43$mm, $w_d = 3.5$mm, $\varepsilon_{r,d} = 23$, $h_d = 0.4$mm, and $m_{s,d} = 0.5$mm for the CPDA and $L_d = 43$mm, $w_d = 3.5$mm, $h_s = 0.48$mm, $\varepsilon_{r,s} = 21$, $m_{s,s} = 0.1$mm, and $H_{w,s} = 0.5$mm for the CGCSA. Figure 11(b) shows the reflection coefficients of the CPDA and the CGCSA, respectively. The CPDA operates near 3.10 GHz and the CPDA cloaks at 3.25 GHz; the cloaked frequency of the CPDA is the operating frequency of the CGCSA, whereas the cloaked frequency of the CGCSA is the operating frequency of the CPDA. Here, the cloaked frequency for the two (complementary) cloaked antennas is the frequency where scattering is canceled. Figure 11(c) shows the corresponding 2D radar cross-section (2D-RCS) for both (complementary) cloaked antennas. The 2D-RCS is a function of frequency; the cloaked frequency of the cloaked antenna is lower across the spectrum: 3.25 GHz for the CPDA and 3.10 GHz for the CGCSA. However, the 2D-RCS characteristic is as functions of frequency, resulting that the cloaked frequency of the cloaked antennas is shown to be lower over the spectrum i.e., at the 3.25 GHz for the CPDA and the 3.10 GHz for the CGCSA. However,
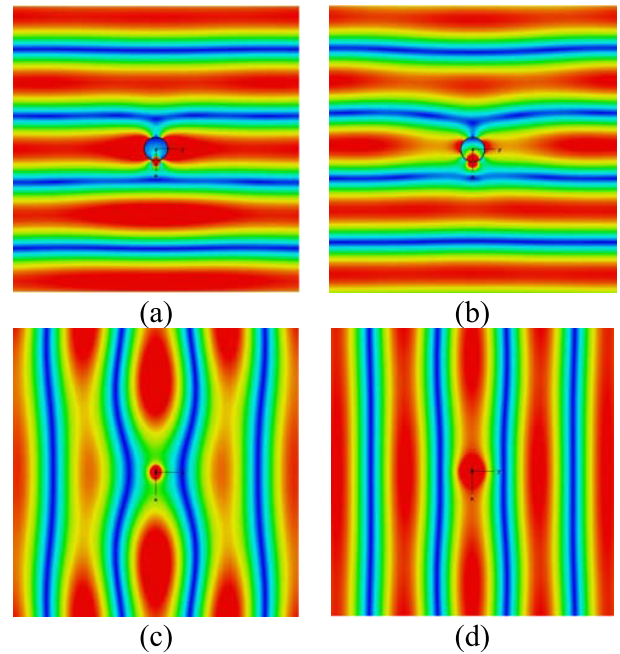

FIGURE 12. Electric field distributions near cloaked antennas with the same dynamic ranges: (a) CGCSA at 3.10 GHz, (b) CGCSA at 3.25 GHz, (c) CPDA at 3.10 GHz, and (d) CPDA at 3.25 GHz.

the 2D-RCS characteristics of the uncloaked antennas vary slightly according to the neighboring frequencies.

The cloaking effect was also explored using the field distributions of Figure 12(a)-(d). The electric field distribution near the antennas was investigated from the perspective of the plane wave incidence. For example, the transverse electric (TE^z) polarized plane wave is typically incident along the negative x-axis for the CGCSA case, as shown in Figure. 12 (a) and (b). When the CGCSA is cloaked, the electric field near the CGCSA at a cloaked frequency of 3.10 GHz is continuous; the CGCSA is completely invisible [Fig. 12(a)]. However, the field near the CGCSA is destructive at an operating frequency of 3.25 GHz, considering the strong scattering from the CSCSA. This observation was confirmed by evaluating the CPDA when the transverse magnetic (TM^z) polarized plane wave was typically incident along the positive y-axis [Figs. 12(c) and (d)]. Extremely destructive field near the CPDA is observed at 3.10 GHz [Fig. 12 (c)], but the field is uniform near the CPDA at the cloaked frequency of 3.25 GHz [Fig. 12 (d)].

The 2D radiation patterns of the complementary cloaked antennas were next explored [Figs. 13(a)-(f)] at the operating and cloaked frequencies. As expected, the cloaked CPDA and CGCSA antennas adequately radiated power at their cloaked frequencies but poorly radiated power at their cloaked frequencies. These results are in good agreement with the cloaking effects observed in previous studies [1], [2], [3], [4], [7].

B. CO-POLARIZED, COUPLED COMPLEMENTARY ANTENNAS
First, we thoroughly investigated the cloaking effects of complementary antennas by placing the two antennas very close
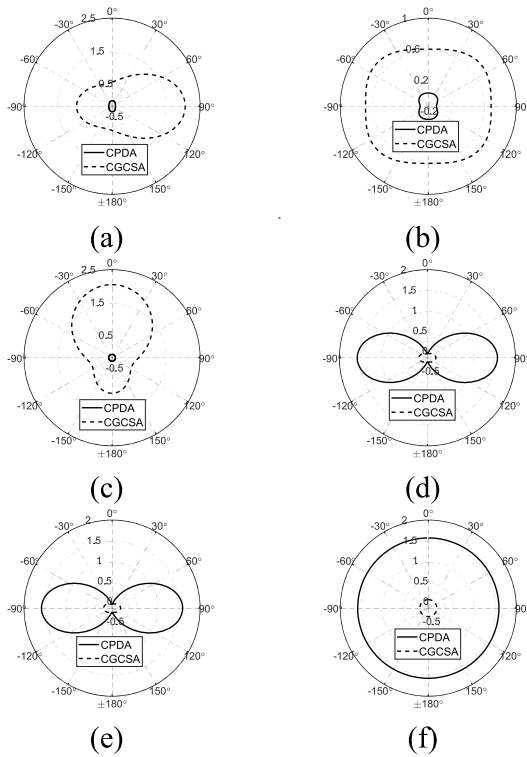
FIGURE 13. Two-dimensional radiation patterns of complementary cloaked antennas; (a) XOZ-plane ($\phi = 0°$) at 3.25 GHz; (b) YOZ-plane ($\phi = 90°$) at 3.25 GHz; (c) XOY-plane ($\theta = 90°$) at 3.25 GHz; (d) XOZ-plane ($\phi = 0°$) at 3.10 GHz; (e) YOZ-plane ($\phi = 90°$) at 3.10 GHz; (f) XOY-plane ($\theta = 90°$) at 3.10 GHz.
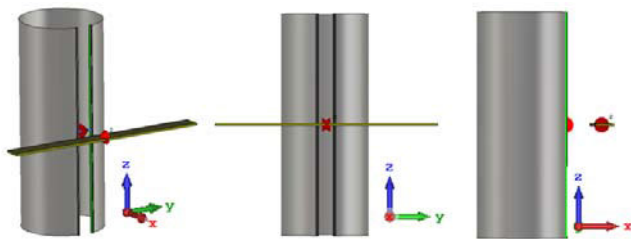

FIGURE 14. Configuration of the co-polarized, coupled complementary antennas: two complementary antennas were placed adjacent ($\lambda_0/15$) and distant ($\lambda_0/2$).

FIGURE 15. Investigation of the cloaking effects for complementary structures with co-polarized coupled cases: (a) scattering parameters with $\lambda_0/15$ distance apart case, (b) total efficiency with $\lambda_0/15$ distance apart case, (a) scattering parameters with $\lambda_0/2$ distance apart case, (b) total efficiency with $\lambda_0/2$ distance apart case.

distance ($\lambda_0/15$) and then very distant from each other ($\lambda_0/2$, where λ_0 is the wavelength at 3.17 GHz). The polarizations of the two complementary antennas were precisely interchanged in the co-polarized coupled configuration [Fig. 14]. This configuration was maintained when the complementary antennas were both uncloaked and cloaked.

Figure 15(a) and (d) shows the characteristics of the co-polarized coupled cases in terms of scattering parameters and total efficiency. Figure 15(a) and (c) shows that the coupling coefficient (S_{21} or S_{12}) of the uncloaked coupled case is approximately −5 dB when the antenna are close but −18 dB when they are distant at approximately 3.10 GHz and 3.25 GHz, coupling is strong between uncloaked coupled antennas. The properties of both antennas are considerably
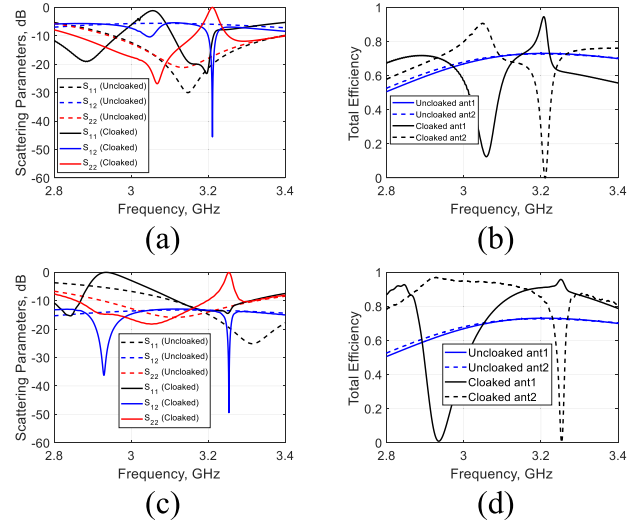
affected by the neighboring antenna, compromising antenna-matching; and the radiation pattern, gain, and efficiency.

Cloaking significantly reduced coupling when the antennas were both adjacent and distant because cloaking created reverse fields that eliminated the scattering fields. In the CPDA, a metasurface anti-phase current canceled the unwanted field. The reverse electric and magnetic fields around the CGCSA slot facilitated scattering cancellation.

The total efficiencies of the co-polarized, coupled complementary antennas are shown in Figure 15(b) and (d) when the antennas were close and distant, respectively. The efficiency of the uncloaked antennas was approximately 70%, but the efficiency of the cloaked antenna was 90 %.

The 2D linear radiation patterns on each principle plane [Figs. 16(a)-(f)] were also explored in terms of the gains provided by co-polarized coupling. The CGCSA was excited in the transmit mode (i.e., at 3.25 GHz) in presence of its dual CPDA structure. The radiation patterns were severely distorted when the complementary antenna was uncloaked at either distance. However, the radiation patterns of the cloaked complementary antenna were in good agreement with the radiation patterns of the isolated case at both distances. Thus, the patterns of all reference planes fully recovered when the complementary antenna was cloaked, even at sub-wavelength separation distance. Scattering cancellation was effective.

C. CROSS-POLARIZED, COUPLED COMPLEMENTARY ANTENNAS

The cross-polarized (X-pol.) coupled characteristics were explored as shown in Figure 17. The two complementary antenna were placed parallel to the z-axis; ports 1 and 2 were connected to the cylindrically grounded slot antenna and the dipole antenna, respectively. We explored both the cloaked
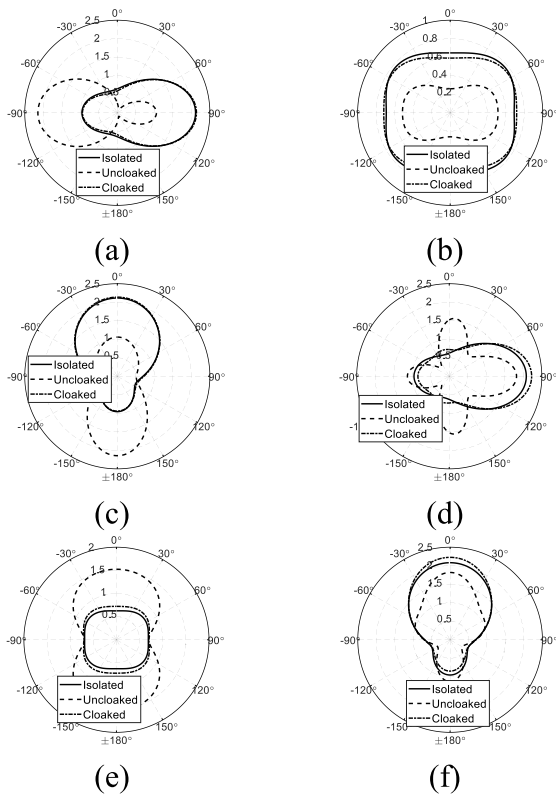
FIGURE 16. Two-dimensional radiation patterns for the co-polarized coupled configurations at 3.25 GHz; (a) XOZ-plane ($\phi = 0°$) at $\lambda_0/15$; (b) YOZ-plane ($\phi = 90°$) at $\lambda_0/15$; (c) XOY-plane ($\theta = 90°$) at $\lambda_0/15$; (d) XOZ-plane ($\phi = 0°$) at $\lambda_0/2$; (e) YOZ-plane ($\phi = 90°$) at $\lambda_0/2$; and (f) XOY-plane ($\theta = 90°$) at $\lambda_0/2$.
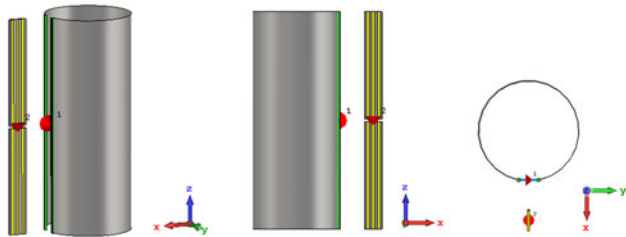

FIGURE 17. Configuration of the cross-polarized (X-pol.) coupled complementary antennas: two complementary antennas are closely spaced with near distance of $\lambda_0/15$ and separated with far distance of $\lambda_0/2$.

FIGURE 18. Characteristics of the cross-polarized (X-pol.), coupled complementary antennas: (a) scattering parameters at $\lambda_0/15$; (b) total efficiency at $\lambda_0/15$; (c) scattering parameters at $\lambda_0/2$; (d) total efficiency at $\lambda_0/2$.

and uncloaked coupled scenarios by evaluating the scattering parameters and total efficiency as a function of frequency.

Figure 18 (a)-(d) shows the performances. Figure 18 (a) and (c) shows that the coupling level (transmission coefficient, S_{12}) of the uncloaked, cross-polarized complementary structure was constant at approximately -130 dB with respect to frequency at a distance of $\lambda_0/15$ and approximately -200 dB at $\lambda_0/2$. However, the coupling level of the cloaked case was < -160 dB at $\lambda_0/15$ but was dramatically decoupled at the cloaked frequency because the total efficiencies [Fig. 18(b) and (d)] show that the efficiency is zero for the cloaked coupled case in cross-polarized configuration
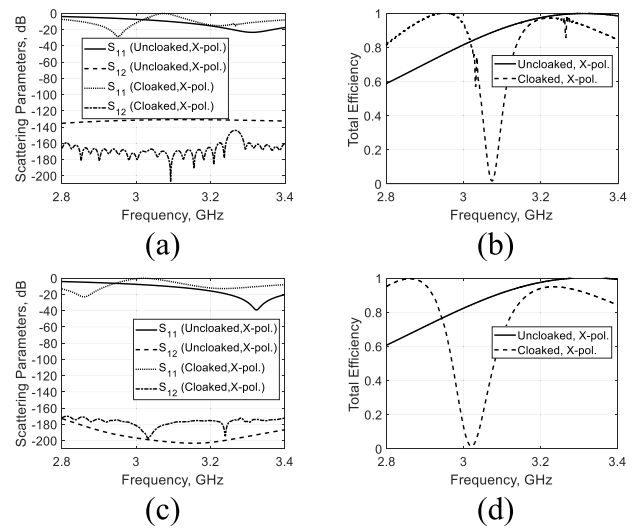
but approximately 90 % at the cloaked frequency for the uncloaked coupled case, indicating substantial coupling.

IV. CONCLUSION

We explored complementary cloaked antennas in terms of decoupling and cloaking. Planar, printed metallic antennas can cloak at any chosen frequency. We developed a cloaked slot antenna with a planar metasurface around the edge. The CPDA and the CGCSA were numerically explored by designing a metasurface that can cloak at a specific frequency and then cancel scattering. We performed detailed parametric studies of both the CPDA and the CGCSA to facilitate the selection of parameters at a desired cloaked frequency. The cloaking and decoupling phenomena of the complementary antennas were intensively explored in terms of reflection coefficient, total efficient, field distributions, and radiation patterns when the antennas were adjacent and distant.

REFERENCES

[1] H. M. Bernety and A. B. Yakovlev, "Reduction of mutual coupling between neighboring strip dipole antennas using confocal elliptical metasurface cloaks," *IEEE Trans. Antennas Propag.*, vol. 63, no. 4, pp. 1554–1563, Apr. 2015.

[2] G. Moreno, A. B. Yakovlev, and H. M. Bernety, "Wideband elliptical metasurface cloaks in printed antenna technology," *IEEE Trans. Antennas Propag.*, vol. 66, no. 7, pp. 3512–3525, Jul. 2018.

[3] G. Moreno, H. M. Bernety, and A. B. Yakovlev, "Reduction of mutual coupling between strip dipole antennas at terahertz frequencies with an elliptically shaped graphene monolayer," *IEEE Antennas Wireless Propag. Lett.*, vol. 15, pp. 1533–1536, 2015.

[4] D. Lee and A. B. Yakovlev, "Metasurface cloaks to decouple closely spaced printed dipole antenna arrays fed by a microstrip-to-balanced transmission-line transition," *IEEE Access*, vol. 9, pp. 128209–128219, 2021.

[5] J. C. Soric, R. Fleury, A. Monti, A. Toscano, F. Bilotti, and A. Alù, "Controlling scattering and absorption with metamaterial covers," *IEEE Trans. Antennas Propag.*, vol. 62, no. 8, pp. 4220–4229, Aug. 2014.

[6] D. Lee, "Study on the pulse characteristics of cloaked cylindrical objects with pulse radar technique," *AEU-Int. J. Electron. Commun.*, vol. 146, Mar. 2022, Art. no. 154103.

[7] D. Lee, "Study of metasurface coated bowtie antenna to decouple closely coupled arrays," *AIP Adv.*, vol. 12, Aug. 2022, Art. no. 115108.

[8] H. M. Bernety, A. B. Yakovlev, H. G. Skinner, S.-Y. Suh, and A. Alù, "Decoupling and cloaking of interleaved phased antenna arrays using elliptical metasurfaces," *IEEE Trans. Antennas Propag.*, vol. 68, no. 6, pp. 4997–5002, Jun. 2020.

[9] A. Alù and N. Engheta, "Achieving transparency with plasmonic and metamaterial coatings," *Phys. Rev. E, Stat. Phys. Plasmas Fluids Relat. Interdiscip. Top.*, vol. 72, no. 1, Jul. 2005, Art. no. 016623.

[10] F. Bilotti, S. Tricarico, and L. Vegni, "Plasmonic metamaterial cloaking at optical frequencies," *IEEE Trans. Nanotechnol.*, vol. 9, no. 1, pp. 55–61, Jan. 2010.

[11] A. Alù, D. Rainwater, and A. Kerkhoff, "Plasmonic cloaking of cylinders: Finite length, oblique illumination and cross-polarization coupling," *New J. Phys.*, vol. 12, no. 10, Oct. 2010, Art. no. 103028.

[12] H. Chen, C. T. Chan, and P. Sheng, "Transformation optics and metamaterials," *Nature Mater.*, vol. 9, no. 5, pp. 387–396, May 2010.

[13] A. Vakil and N. Engheta, "Transformation optics using graphene," *Science*, vol. 332, no. 6035, pp. 1291–1294, Jun. 2011.

[14] D.-H. Kwon and D. H. Werner, "Restoration of antenna parameters in scattering environments using electromagnetic cloaking," *Appl. Phys. Lett.*, vol. 92, no. 11, Mar. 2008, Art. no. 113507.

[15] J. B. Pendry, D. Schurig, and D. R. Smith, "Controlling electromagnetic fields," *Science*, vol. 312, pp. 1780–1782, Jun. 2006.

[16] J. Li and J. B. Pendry, "Hiding under the carpet: A new strategy for cloaking," *Phys. Rev. Lett.*, vol. 101, Nov. 2008, Art. no. 203901.

[17] P. Alitalo, O. Luukkonen, L. Jylha, J. Venermo, and S. A. Tretyakov, "Transmission-line networks cloaking objects from electromagnetic fields," *IEEE Trans. Antennas. Propag.*, vol. 56, no. 2, pp. 416–424, Feb. 2008.

[18] P. Alitalo, J. Vehmas, and S. Tretyakov, "Reduction of antenna blockage with a transmission-line cloak," in *Proc. 5th Eur. Conf. Antennas Propag. (EUCAP)*, Apr. 2011, pp. 2399–2402.

[19] J. Vehmas, P. Alitalo, and S. A. Tretyakov, "Experimental demonstration of antenna blockage reduction with a transmission-line cloak," *IET Microw., Antennas Propag.*, vol. 6, no. 7, pp. 830–834, 2012.

[20] S. Tretyakov, P. Alitalo, O. Luukkonen, and C. Simovski, "Broadband electromagnetic cloaking of long cylindrical objects," *Phys. Rev. Lett.*, vol. 103, Sep. 2009, Art. no. 103905.

[21] Y. R. Padooru, A. B. Yakovlev, P.-Y. Chen, and A. Alù, "Analytical modeling of conformal mantle cloaks for cylindrical objects using subwavelength printed and slotted arrays," *J. Appl. Phys.*, vol. 112, no. 3, 2012, Art. no. 034907.

[22] S. Pawar, H. G. Skinner, S.-Y. Suh, and A. B. Yakovlev, "Metasurface cloaks for reduction of mutual coupling in slot antennas at C-band frequencies," in *Proc. IEEE Int. Symp. Antennas Propag. USNC-URSI Radio Sci. Meeting (AP-S/URSI)*, Jul. 2022, pp. 966–967.

[23] S. Pawar, H. G. Skinner, S.-Y. Suh, and A. B. Yakovlev, "Cloaking of slot antennas at C-band frequencies using elliptical metasurface cloaks," *IEEE Antennas Wireless Propag. Lett.*, vol. 21, no. 11, pp. 2171–2175, Nov. 2022.

[24] (2019). *CST Microwave Studio CST*. [Online]. Available: http://www.cst.com

DOOJIN (JIN) LEE (Member, IEEE) received the Ph.D. degree in biomedical science and engineering from the Gwangju Institute of Science and Technology (GIST), Gwangju, South Korea, in 2017.

He was a Postdoctoral Fellow with the University of Waterloo (UW), Waterloo, ON, Canada, from 2017 to 2019; and the Electroscience Laboratory (ESL), Ohio State University (OSU), Columbus, OH, USA, from 2019 to 2020, where he was extensively involved in several projects, including the development of a low-profile, global navigation satellite system (GNSS) receiver and an ultrawideband, noncontact, ground-penetrating radar antenna. From February 2020 to September 2020, he was a Research Associate with the Department of Electrical Engineering, University of Mississippi (Ole Miss), Oxford, MS, USA. From October 2020 to September 2022, he was a Senior Researcher with the Naval Combat Systems Project Management Office (PMO), Maritime Technology Research Institute, Agency for Defense Development (ADD), Changwon, South Korea. He joined as an Assistant Professor with the Department of Electrical, Electronic, and Control Engineering, Changwon National University (CWNU), Changwon, in 2022. His research interests include ultrawideband-based, impulse-like, radiating antenna design; pulsed radar signal processing; microwave imaging for biomedical and industrial applications; GNSS antenna receiver designs; and the fundamental study of electromagnetic cloaking and decoupling theory utilizing mantle metasurfaces.

● ● ●